

# Normal Mode Splitting and Force Sensing in Cavity Magnomechanical System

Ghaisud Din,<sup>1</sup> Muqaddar Abbas,<sup>1</sup> and Pei Zhang<sup>1</sup>

<sup>1</sup>*Ministry of Education Key Laboratory for Nonequilibrium Synthesis and Modulation of Condensed Matter, Shaanxi Province Key Laboratory of Quantum Information and Quantum Optoelectronic Devices, School of Physics, Xi'an Jiaotong University, Xi'an 710049, China*

(Dated: December 2, 2024)

In this study, we investigate the dynamics of system composed of a single cavity consisting of an optical parametric amplifier (OPA) and a YIG sphere influenced by a bias magnetic field. This bias field leads to magnetostrictive effects on magnon modes that induces phonons. We investigate the position fluctuation spectrum  $S_b(\omega)$  and the output field spectrum  $S_{\text{out}}(\omega)$ , finding that at  $G = 0$ , the system displays a single peak, indicative of weak coupling between the optical and phononic modes. As  $G$  increases (e.g.,  $G = 0.1\kappa_a, 0.2\kappa_a, 0.4\kappa_a$ ), we observe a transition to double peak, which reflects stronger coupling in the vicinity of cavity along with phonon modes that leads to normal mode splitting (NMS) in cavity magnomechanic system. Furthermore, we examine that the OPA amplifies the  $Y$  quadrature while squeezing the  $X$  quadrature of the output field spectrum. This sensitive behavior results in a more pronounced splitting in the  $Y$ -quadrature spectra compared to the  $X$  quadrature. Our findings emphasize the essential role of the OPA in adjusting the interaction strength between the optical and phononic modes as well as underscore the importance of quadrature analysis in characterizing the system's response. NMS mechanism open avenues for advanced applications in quantum sensing and information processing, highlighting the potential for tunable devices in emerging quantum technologies.

## I. Introduction

Cavity optomechanical system is a setup that combines two types of resonators: optical (which involves light) and mechanical (which involves physical vibrations). These systems are studied because they can be used to detect extremely small changes, making them useful for quantum sensing: a method of measuring things with extreme precision at the quantum level. Additionally, they provide a way to explore and test aspects of quantum theory, which deals with the behavior of particles at the smallest scales, where the laws of classical physics no longer apply. Researchers are interested in these systems because of their potential to push the boundaries of our understanding and applications of quantum phenomena [1].

Scientists have successfully cooled a mechanical oscillator to its quantum ground state using various techniques. This ground state represents the lowest energy level an object can attain in quantum mechanics, minimizing its motion so that quantum effects become predominant. Achieving this milestone is significant, as it enables researchers to investigate the oscillator's behavior within a purely quantum framework [2–6] which allows the researchers to observe the phenomenon like normal mode splitting [7]. Normal mode splitting in optomechanics refers to the phenomenon that occurs when two or more coupled oscillators, such as a mechanical oscillator and a cavity field, interact and create distinct vibrational modes. When the coupling between these oscillators is strong, the energy levels split into separate modes, allowing for a clearer distinction between their behaviors. This is a hallmark of strong coupling between the optical and mechanical elements [8] as well as in a weak coupling regime [9] which is the key to search for the coherent quantum control [10, 11]. Researchers has

already demonstrated the normal mode splitting experimentally for an atom-cavity system [12], and by considering quantum-dot in a micro cavity [13]. Furthermore, various techniques and methods are applied to optomechanical systems to see the effects on normal mode splitting like, the output spectrum from an optomechanical system shows a double-peak structure by considering the Gain of the optical parametric amplifier [7]. In addition normal mode splitting is experimentally investigated in the optical domain [8] which provide strong interaction between cavity photons and a mechanical resonator.

Moreover, it has been shown that a medium with strong Kerr nonlinearity inside the cavity suppresses normal mode splitting due to the photon blockade effect [14] offering a method to coherently control the micromirror's dynamics. More research regarding normal mode splitting in cavity optomechanical system can be found in these references [15–23].

On the other hand a developing field, cavity magnomechanics is an emerging area that investigates the interactions among magnons, cavity photons, and mechanical vibrations (phonons) in hybrid quantum systems, usually contained within a cavity [24, 25]. Magnons are quanta of spin waves, collective excitations within a magnetic material. These arise from the coherent precession of electron spins in a magnetized medium. Magnon-based systems are often realized using materials like yttrium iron garnet (YIG), which exhibit strong magnon-photon and magnon-phonon coupling. In cavity magnonics experiment demonstrated strong coupling between magnons and photons in YIG-microwave cavity systems and are sensitive against temperature [26, 27]. In addition, a theoretical study on magnon-polariton formation and strong coupling mechanisms in hybrid systems are investigated [28]. Cavity magnomechanics operates effectively

in the quantum regime at millikelvin temperatures, where thermal noise is significantly reduced, allowing quantum effects to dominate. This low-temperature environment is crucial for exploring and exploiting the interactions between magnons, cavity photons, and phonons. One of the key applications is in developing tunable microwave filters and amplifiers, which can selectively enhance certain frequency signals, making them valuable for telecommunications and signal processing [29]. Additionally, cavity magnomechanics offers the potential for long-lifetime quantum memories, which can store and retrieve quantum information over extended periods without significant loss, a critical feature for quantum computing and secure information transfer [30]. Furthermore, the ability to convert microwave signals to optical frequencies paves the way for integrating microwave-based quantum systems with existing optical technologies, facilitating advancements in quantum communication and networking [31]. These applications highlight the transformative potential of cavity magnomechanics in advancing quantum technology.

In the past, extensive research in cavity magnomechanics has investigated phenomena such as magnomechanically induced transparency [25], generating grating in cavity magnomechanics [32], squeezed states of magnon and phonons [33], coherent State transfer between magnons, photons, and phonons [34], magnon-photon-phonon entanglement [35–37], fast light generation [38], magnetic chaos [39] and phonon lasing is proposed based on three-mode cavity magnomechanical system [40], as well as the dynamics of backaction in this field [41]. However, the detailed exploration of normal mode splitting in cavity magnomechanics has been limited, which is the focus of the current study.

In this paper, we investigate the normal mode splitting behavior of the cavity field and mechanical vibrations. While previous studies have extensively addressed magnon-photon and magnon-phonon couplings in YIG-based systems, there is a notable gap in the explicit examination of normal mode splitting between phonons and photons in laser-driven cavities under a bias magnetic field. This integration of techniques and phenomena could be particularly beneficial for both scientific understanding and potential applications.

The paper is structured as follows: Section II presents a detailed discussion of the model and its corresponding Hamiltonian, laying the foundation for the subsequent analyses. In section III we will be about to discuss the results of this paper. Finally, Section IV serves as the conclusion, summarizing the findings and providing a wrap-up of the study's key insights and implications.

## II. MODEL AND HAMILTONIAN

We analyze a single cavity system shown in Fig.1, on which a laser is applied from the left which creates the electromagnetic field inside the cavity. In addition yttrium iron garnet YIG sphere is placed inside the cavity, which is driven by an external bias magnetic field

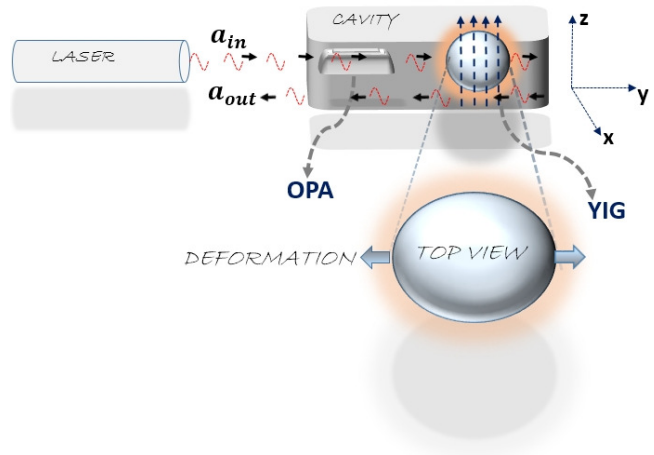


FIG. 1. Representation of the model, illustrating the laser-driven single cavity from the left. An OPA and the YIG sphere are placed inside the cavity where the YIG is influence due to a bias magnetic field shown by the arrows in the z direction.

as shown by the arrows in the z direction. When a uniform magnetic field is applied along the z-direction to a YIG sphere, it stimulates the magnon modes, which are quantized spin waves in the material. This excitation occurs due to the alignment of spins under the influence of the magnetic field, creating fluctuations in magnetization. These magnon modes interact with the electromagnetic field within a cavity through magnetic dipole interactions. As the magnon modes are excited, the variations in magnetization can induce changes in the lattice structure of the YIG sphere, a phenomenon known as magnetostriction. This effect results from the coupling between the magnetic and mechanical properties of the material. The resulting magnetostrictive forces cause the YIG sphere to vibrate, leading to the establishment of magnon-phonon interactions [42]. The Hamiltonian of the total system can be written as

$$\begin{aligned}
 H = & \hbar\Delta_a a^\dagger a + \hbar\omega_b b^\dagger b + \hbar\Delta_m m^\dagger m + \hbar g_{ma}(m^\dagger a + ma^\dagger) \\
 & + \hbar g_{mb} m^\dagger m (b + b^\dagger) + \hbar g_{ap}(a^\dagger b + ab^\dagger) \\
 & + i\hbar G(e^{i\theta} a^{\dagger 2} - e^{-i\theta} a^2) \\
 & + i\Omega(m^\dagger - m) + i\hbar\mathcal{E}(a^\dagger - a) + F_{ext}. \quad (1)
 \end{aligned}$$

The first term in Eq 1 shows the cavity free energy where  $a$   $a^\dagger$  are the annihilation (creation) operator of the cavity modes, while the second term denotes the magnon mode energy with annihilation (creation) operator  $m$   $m^\dagger$ . In the third term Q and P are the dimensionless position and momentum quadratures of the mechanical mode where  $\omega_b$  is the mechanical resonance frequency. The fourth term in Eq 1 shows the interaction of the

magnon mode with the mechanical mode with a coupling parameter  $g_{mb}$  while in the fifth term  $g_{ma}$  represents the coupling parameter for the interaction of the cavity-magnon modes. The last three terms represents the drive magnetic field with Rabi frequency  $\Omega$ , the interaction of the optical parametric amplifier and cavity with Gain  $G$ , and the interaction of the laser source with the cavity. Here we would like to mention that the frequency of the magnons denoted by  $\omega_m$  is determined by two factors, The external bias magnetic field  $H$  applied to the material (YIG) and The gyromagnetic ratio  $\gamma$ , which relates the magnetic moment of a particle to its angular momentum and is a property of the material. The equation  $\omega_m = \gamma H$  shows that as the external magnetic field strength  $H$  increases, the magnon frequency increases proportionally. Here the Rabi frequency  $\Omega$  shows the strength between magnon and the drive magnetic field and can be defined as  $\Omega = \frac{\sqrt{5}}{4}\gamma\sqrt{NB_0}$ .

By employing the Heisenberg equations of motion and incorporating both the damping and noise terms, we derive the quantum Langevin equations in the following form

The terms  $b_{in}$ ,  $a_{in}$ ,  $m_{in}$  in the last of equation 2 are the noise operators for the mechanical, cavity, and magnon modes. Further more the input vacuum noise operator  $b_{in}$ ,  $a_{in}$ ,  $m_{in}$  associated with the mechanical, cavity, and magnon having zero mean value  $\langle b_{in}(t) \rangle = \langle a_{in}(t) \rangle = \langle m_{in}(t) \rangle = 0$ , which obeys the correlation function

$$\langle \delta b_{in}(t) \delta b_{in}^\dagger(t') \rangle = \delta(t - t'),$$

$$\langle \delta a_{in}(t) \delta a_{in}^\dagger(t') \rangle = \delta(t - t'),$$

$$\langle \delta m_{in}(t) \delta m_{in}^\dagger(t') \rangle = \delta(t - t'),$$

The phenomenon of normal mode splitting between photon and phononic vibrations can be understood through the interactions and fluctuations in the system, here a laser, generating a coherent field of photons inside the cavity, while a ferrimagnetic material that can support both magnon spin wave and phonon mechanical vibration modes. The coupling between the magnetic and mechanical properties of the YIG enables the interaction between magnons, phonons, and photons. The cavity field interacts with the phonon modes where the displacement of the YIG material induces changes in the magnetic state, thus affecting the photon field. To analyze how normal mode splitting occurs between photons and phonons, we would like to mention the steady-state configuration where the mean values of the photon and phonon operators are stable.

$$\begin{aligned} \dot{a} = & -(i\Delta_a + \kappa_a)a - ig_{ma}m - ig_{ap}b + \mathcal{E} + 2Ge^{i\theta}a^\dagger \\ & + \sqrt{2\kappa_a}a_{in} \end{aligned}$$

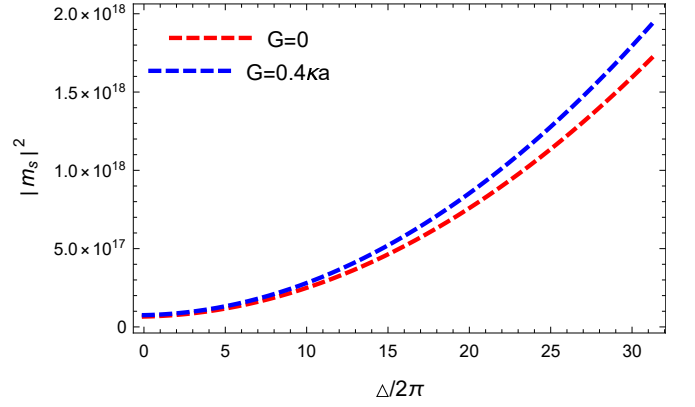


FIG. 2. Magnon number plotted as function of  $\Delta/2\pi$ . All the parameters are the same as shown in table I.

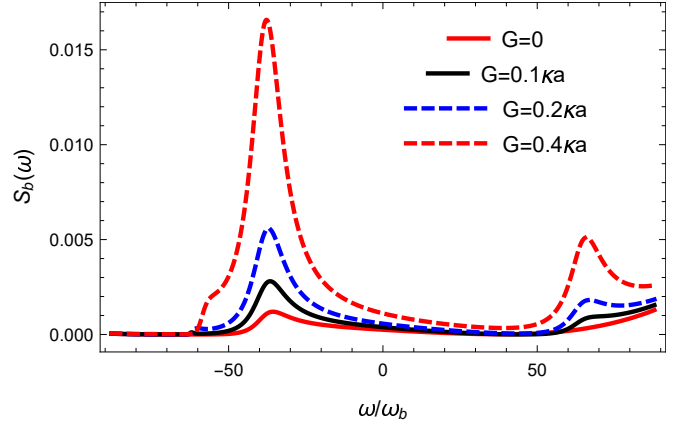


FIG. 3. The spectral density of the fluctuations  $\delta_b(\omega)$  as a function of normalized frequency  $\omega/\omega_b$ , for the same parameters given in table I.

$$\begin{aligned} \dot{a}^\dagger = & -(i\Delta_a + \kappa_a)a^\dagger + ig_{ma}m^\dagger + ig_{ap}b^\dagger + \mathcal{E} + 2Ge^{-i\theta}a \\ & + \sqrt{2\kappa_a}a_{in}^\dagger \\ \dot{m} = & -(i\Delta_m + \kappa_m)m - ig_{ma}a - ig_{mb}m(b + b^\dagger) + \Omega \\ & + \sqrt{2\kappa_m}m_{in} \\ \dot{m}^\dagger = & -(i\Delta_m + \kappa_m)m^\dagger + ig_{ma}a^\dagger + ig_{mb}m^\dagger(b^\dagger + b) + \Omega \\ & + \sqrt{2\kappa_m}m_{in}^\dagger \\ \dot{b} = & -(i\omega_b + \kappa_b)b - ig_{mb}m^\dagger m - ig_{ap}a + \sqrt{2\kappa_b}b_{in} + F_{ext} \\ \dot{b}^\dagger = & -(i\omega_b + \kappa_b)b^\dagger + ig_{mb}mm^\dagger + ig_{ap}a^\dagger + \sqrt{2\kappa_b}b_{in}^\dagger. \end{aligned}$$

Further more the steady-state value plus a small fluctuation around that value is given by

$$a = a_s + \delta a, m = m_s + \delta m, b = b_s + \delta b, \quad (2)$$

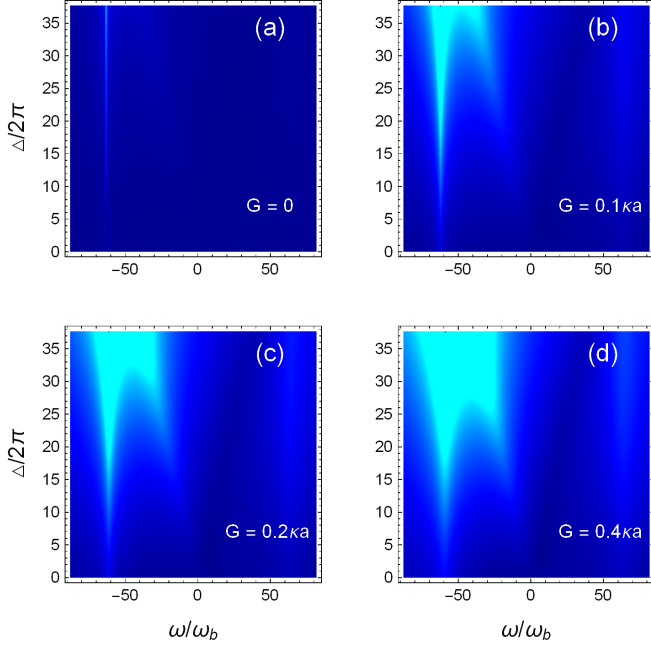


FIG. 4. Density Plot of the spectral density  $S_{out}(\omega)$  of the output field as a function of normalized frequency  $\omega/\omega_b$  and  $\Delta/2\pi$  for the same parameters in table I.

Using equation 4 in equation 2 we get the following equations for the fluctuation operators

$$\begin{aligned}
 \delta\dot{a} &= -(i\Delta_a + \kappa_a)\delta a - ig_{ma}\delta m - ig_{ap}\delta b + 2Ge^{i\theta}\delta a^\dagger \\
 &\quad + \sqrt{2\kappa_a}\delta a_{in} \\
 \delta\dot{a}^\dagger &= -(-i\Delta_a + \kappa_a)\delta a^\dagger + ig_{ma}\delta m^\dagger + ig_{ap}\delta b^\dagger + 2Ge^{-i\theta}\delta a \\
 &\quad + \sqrt{2\kappa_a}\delta a_{in}^\dagger \\
 \delta\dot{m} &= -(i\Delta + \kappa_m)\delta m - ig_{ma}\delta a + \sqrt{2\kappa_m}\delta m_{in} \\
 \delta\dot{m}^\dagger &= -(-i\Delta + \kappa_m)\delta m^\dagger + ig_{ma}\delta a^\dagger + \sqrt{2\kappa_m}\delta m_{in}^\dagger \\
 \delta\dot{b} &= -(i\omega_b + \kappa_b)\delta b - ig_{mb}(\delta m^*m_s + m_s^*\delta m) - ig_{ap}\delta a \\
 &\quad + \sqrt{2\kappa_b}\delta b_{in} + F_{ext} \\
 \delta\dot{b}^\dagger &= -(-i\omega_b + \kappa_b)\delta b^\dagger + ig_{mb}(\delta mm_s^* + m_s\delta m^*) + ig_{ap}\delta a^\dagger \\
 &\quad + \sqrt{2\kappa_b}\delta b_{in}^\dagger
 \end{aligned} \tag{3}$$

Where  $\Delta = \Delta_m + g_{mb}(b_s + b_s^*)$ .

### III. Fluctuation and output spectra

In order to see the normal mode splitting of the phononic and cavity modes, we need to calculate the fluctuation

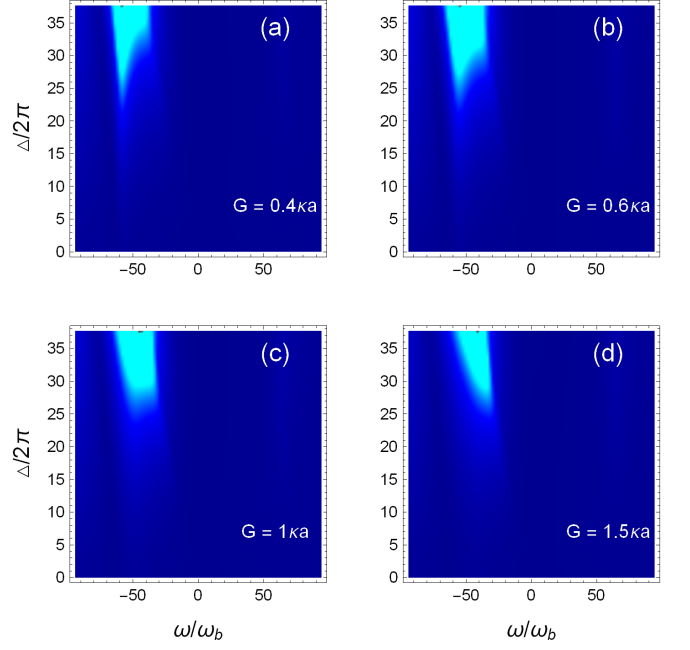


FIG. 5. Density Plot of the quadrature spectral density  $S_X(\omega)$  of the output field as a function of normalized frequency  $\omega/\omega_b$  and  $\Delta/2\pi$  for the same parameters in table I.

tuation  $\delta b(\omega)$ , and  $\delta a(\omega)$ , by using

$$\begin{aligned}
 f(t) &= \frac{1}{2\pi} \int_{-\infty}^{\infty} f(\omega)e^{i\omega t} d\omega \\
 f^\dagger(t) &= \frac{1}{2\pi} \int_{-\infty}^{\infty} f^\dagger(\omega)e^{i\omega t} d\omega
 \end{aligned} \tag{4}$$

and input output relation [43]  $x_{out}(\omega) = \sqrt{2\kappa_x}(\omega) - x_{in}(\omega)$  in equation 5, Where  $x = a$ . Once we solve equation 3 with Fourier transform, the spectrum  $S_b(\omega)$  of the position fluctuation  $\delta_b(\omega)$  of the phononic modes, and the output spectrum  $S_{out}(\omega)$  of the fluctuation  $\delta_a(\omega)$  can be obtained, and is written with a simplified form for simplicity.

$$\begin{aligned}
 S_b(\omega) &= N_1 + \frac{N_2}{A_2 + \zeta_4 A_3} + \frac{(2\kappa_m(N_3)(N_4 + N_5))}{(\eta_1(g_{ma}\zeta_3(A_5) + \zeta_3\zeta_4(A_4)))}, \\
 S_{out}(\omega) &= -\frac{2\zeta_1\zeta_3\zeta_4\kappa_a(\zeta_6 + 2\zeta_1\zeta_3Ge^{i\theta})}{B_1} \\
 &\quad - \frac{4i\zeta_3\zeta_4g_{ap}\sqrt{\kappa_a\kappa_b}^{3/2}\omega\left(\frac{2k_B T}{\omega\hbar} - 1\right)(\zeta_6 + 2\zeta_1\zeta_3Ge^{i\theta})}{B_1\omega b} \\
 &\quad - \frac{\sqrt{2}B_3\sqrt{\kappa_a}}{B_2},
 \end{aligned} \tag{5}$$

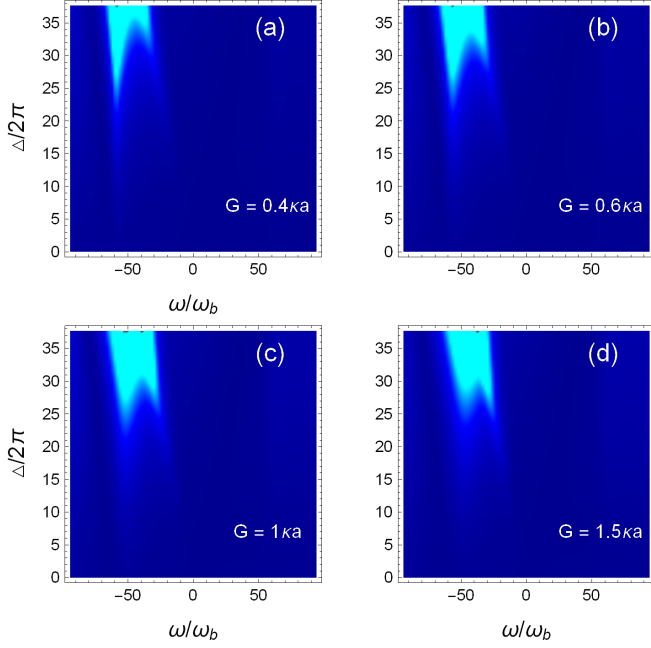


FIG. 6. Density Plot of the quadrature spectral density  $S_Y(\omega)$  of the output field as a function of normalized frequency  $\omega/\omega_b$  and  $\Delta/2\pi$  for the same parameters in table I.

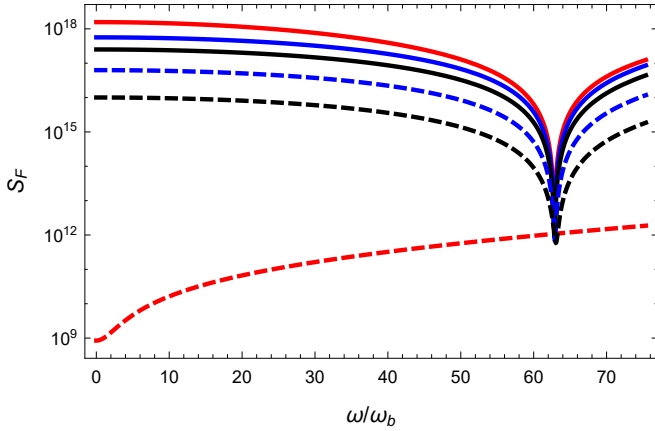


FIG. 7. Force sensitivity  $S_F(\omega)$  as a function of normalized frequency  $\omega/\omega_b$  for the same parameters in table I. The parametric gain for Red, Blue, Black, Blue dashed, Black dashed color lines are  $G = 0, 0.2\kappa_a, 0.3\kappa_a, 0.4\kappa_a, 0.46\kappa_a$ , while for the Red dashed is  $G = 0.5\kappa_a$ , which represents the combined effects from the noises.

#### IV. Quadrature spectra

To quantify the fluctuation of the X and Y quadrature of the output field, we need to define the spectrum of each quadrature, The spectrum of the X quadrature is given by:

$$S_X(\omega) = \langle \delta X_{\text{out}}(\omega) \delta X_{\text{out}}(-\omega) \rangle \quad (6)$$

The spectrum of the Y quadrature is given by:

$$S_Y(\omega) = \langle \delta Y_{\text{out}}(\omega) \delta Y_{\text{out}}(-\omega) \rangle \quad (7)$$

Where

$$S_X(\omega) = (D_1 + \bar{D})(D + \bar{D}_1) - \frac{2\kappa_b(-2k_B T + \omega\hbar)(C_1 + \bar{C})(C + \bar{C}_1)}{\omega_b\hbar}, \quad (8)$$

$$S_Y(\omega) = -(D_1 - \bar{D})(D - \bar{D}_1) + \frac{2\kappa_b(-2k_B T + \omega\hbar)(C_1 - \bar{C})(C - \bar{C}_1)}{\omega_b\hbar}, \quad (9)$$

#### V. Normal mode Splitting and Eigenvalues

By using the quadrature of the cavity-magnon-phonon modes  $\delta x = \delta a + \delta a^\dagger$ ,  $\delta y = i(\delta a^\dagger - \delta a)$ ,  $\delta X = \delta m + \delta m^\dagger$ ,  $\delta Y = i(\delta m^\dagger - \delta m)$ ,  $\delta v = \delta b + \delta b^\dagger$ ,  $\delta w = i(\delta b^\dagger - \delta b)$  with input noise  $\delta x_{in} = \delta a_{in} + \delta a_{in}^\dagger$ ,  $\delta y_{in} = i(\delta a_{in}^\dagger - \delta a_{in})$ ,  $\delta X_{in} = \delta m_{in} + \delta m_{in}^\dagger$ ,  $\delta Y_{in} = i(\delta m_{in}^\dagger - \delta m_{in})$ ,  $\delta v_{in} = \delta b_{in} + \delta b_{in}^\dagger$ ,  $\delta w_{in} = i(\delta b_{in}^\dagger - \delta b_{in})$  in equation 4 and can be written as

$$\begin{pmatrix} \delta \dot{a} \\ \delta \dot{a}^\dagger \\ \delta \dot{m} \\ \delta \dot{m}^\dagger \\ \delta \dot{b} \\ \delta \dot{b}^\dagger \end{pmatrix} = Z + \begin{pmatrix} \sqrt{2\kappa_a} \delta a_{in} \\ \sqrt{2\kappa_a} \delta a_{in}^\dagger \\ \sqrt{2\kappa_m} \delta m_{in} \\ \sqrt{2\kappa_m} \delta m_{in}^\dagger \\ \sqrt{2\kappa_b} \delta b_{in} \\ \sqrt{2\kappa_b} \delta b_{in}^\dagger \end{pmatrix} \quad (10)$$

In the above matrix the transpose of the fluctuation

TABLE I. Experimental Parameters[24]

Parameter	Symbol	Value
cavity-magnon coupling strength	$g_{ma}$	$2\pi \times 1$ MHz
cavity-phonon coupling strength	$g_{ap}$	$2\pi \times 1$ MHz
magnon-phonon coupling strength	$g_{mb}$	$2\pi \times 0.2$ Hz
mechanical frequency	$\omega_b$	$2\pi \times 10$ MHz
cavity dissipation rate	$\kappa_a$	$2\pi \times 1$ MHz
magnon dissipation rate	$\kappa_m$	$2\pi \times 1$ MHz
phonon dissipation rate	$\kappa_b$	$2\pi \times 10^2$ Hz
Temperature	$T$	10 mK
Power	$P$	10 mW

vectors of the first column and second column can be expressed as

$$(\delta x, \delta y, \delta X, \delta Y, \delta v, \delta w)$$

$$(\sqrt{2\kappa_a} \delta x_{in}, \sqrt{2\kappa_a} \delta y_{in}, \sqrt{2\kappa_m} \delta X_{in}, \sqrt{2\kappa_m} \delta Y_{in}, \sqrt{2\kappa_b} \delta v_{in}, \sqrt{2\kappa_b} \delta w_{in})$$

where Z is given as,



$$Z = \begin{pmatrix} -\kappa_a + 2G\cos\theta & \Delta_a + 2G\sin\theta & 0 & g_{ma} & 0 & g_{ap} \\ -\Delta_a + 2G\sin\theta & -\kappa_a - 2G\cos\theta & -g_{ma} & 0 & -g_{ap} & 0 \\ 0 & g_{ma} & -\kappa_m & \Delta & 0 & 0 \\ -g_{ma} & 0 & -\Delta & -\kappa_m & 0 & 0 \\ 0 & g_{ma} & 0 & -g_{mb}(m_s - m_s^*) & -\kappa_b & \omega_b \\ -g_{ap} & 0 & -g_{mb}(m_s + m_s^*) & 0 & -\omega_b & -\kappa_b \end{pmatrix}$$

Further more, the Routh-Hurwitz criterion [44] is a method for analyzing the stability of a systems, providing a systematic approach to determining whether all eigenvalues of the characteristic polynomial have negative real parts. This criterion entails constructing the Routh-Hurwitz table from the coefficients of the characteristic polynomial, where the stability of the system is assessed by examining the signs of the first column values. Specifically, a system is stable if all entries in the first column of the Routh-Hurwitz table are positive. This condition indicates that the corresponding characteristic polynomial has no roots in the right half of the complex plane, confirming that all eigenvalues possess negative real parts. The stability conditions can be written as

$$\begin{aligned} &\hookrightarrow 2g_{ap}^3 g_{ma} g_{mb} m_s^* \Delta - g_{ap}^4 (\kappa_m^2 + \Delta^2) + 2g_{ap} g_{ma} g_{mb} \\ &\quad m_s^* (g_{ma}^2 \omega_b + \kappa_a \kappa_m \omega_b + \kappa_a \kappa_b \Delta + \kappa_b \kappa_m \Delta_a - \omega_b \Delta \Delta_a) \\ &\quad - g_{ap}^2 (g_{ma}^2 (g_{mb}^2 (-m_s^2 + m_s^2)) + 2(\kappa_b \kappa_m + \omega_b \Delta)) \\ &\quad + 2(\kappa_m^2 + \Delta^2)(\kappa_a \kappa_b - \omega_b \Delta_a) - (\kappa_b^2 + \omega_b^2)(g_{ma}^4 \\ &\quad + 2g_{ma}^2 (\kappa_a \kappa_m - \Delta \Delta_a) - (\kappa_m^2 + \Delta^2)(4G^2 - \kappa_a^2 - \Delta_a^2)) \\ &\quad - 4G g_{ap} g_{ma} g_{mb} m_s ((\kappa_m \omega_b - \kappa_b \Delta) \cos\theta \\ &\quad + (\kappa_b \kappa_m + \omega_b \Delta) \sin\theta) > 0 \\ &\hookrightarrow 2(\kappa_a + \kappa_b + \kappa_m) > 0 \end{aligned} \quad (11)$$

## VI. Results and discussion

We utilize the experimentally feasible parameters listed in Table I to analyze the normal mode splitting phenomena of the phononic and cavity field modes in a YIG-cavity system. Our proposed setup includes an optical parametric amplifier (OPA), which amplifies quantum fluctuations within the system. The gain  $G$  of the OPA determines the level of amplification. As  $G$  increases, the effective interaction strength of the system is enhanced, affecting the energy exchange among the optical cavity modes, magnons, and mechanical modes (phonons). The average magnon number  $m_s$ , representing the magnon population in the system, rises as the gain  $G$  of the OPA increases. This means that more photons are amplified within the cavity, leading to a greater magnon population due to stronger interactions between the cavity and magnon modes. This effect is shown in Fig.2, where  $m_s$  is plotted as a function of  $\Delta/2\pi$ . The interaction strength is enhanced when  $G = 0.4\kappa_a$  as compared to  $G = 0$ . Furthermore, Figure 3 illustrates the significant impact of the optical parametric amplifier (OPA) gain  $G$  on the phonon fluctuation spectrum  $S_b(\omega)$ . The OPA enables controllable amplification of the cavity field, which subsequently influences the coupling between the cavity modes and the phonon modes. By affecting the amplitude and fluctuation dynamics of the cavity mode, the OPA alters the effective interaction between the optical cavity and the phonon modes.

Moreover, in Fig.3, the effect of the optical parametric amplifier OPA gain  $G$  on the phonon fluctuation spectrum  $S_b(\omega)$  has been examined, that is quite significant. The OPA introduces a controllable amplification of the

$$\begin{aligned} &\hookrightarrow -4G^2 \kappa_a + g_{ma}^2 \kappa_a + \kappa_a^3 + 4\kappa_a^2 \kappa_b + 4\kappa_a \kappa_b^2 + \kappa_b^3 \\ &\quad + g_{ap}^2 (\kappa_a + \kappa_b) + g_{ma}^2 \kappa_m + 4\kappa_a^2 \kappa_m + 8\kappa_a \kappa_b \kappa_m \\ &\quad + 4\kappa_b^2 \kappa_m + 4\kappa_a \kappa_m^2 + 4\kappa_b \kappa_m^2 + \kappa_m^3 + \kappa_b \omega_b^2 \\ &\quad + \kappa_m \Delta^2 + \kappa_a \Delta_a^2 / (\kappa_a + \kappa_b + \kappa_m) > 0 \\ &\hookrightarrow \frac{(\kappa_a + \kappa_b + \kappa_m) E_1 \left( - \left( \frac{(\kappa_a + \kappa_b + \kappa_m) E_7 E_1}{E_4} \right) + \frac{E_3}{E_1} \right)}{E_4 \left( - \frac{E_2}{2E_4} \right)} > 0 \\ &\hookrightarrow E_4 (E_1 (2E_8 (\kappa_a + \kappa_b + \kappa_m) - 2E_6 / 2E_4) + \\ &\quad 2E_4 E_6 (-1/\kappa_a) - \kappa_b - \kappa_m) + 2E_7 (\kappa_a + \kappa_b \\ &\quad + \kappa_m) / (E_1 (\kappa_a + \kappa_b + \kappa_m)) > 0 \end{aligned}$$

cavity field, which in turn affects the coupling between the cavity modes and the phonon modes. The OPA modifies the effective interaction between the optical cavity and the phonon modes by influencing the cavity mode's amplitude and fluctuation dynamics. This interaction is mediated through the  $g_{\text{ap}}$  coupling between the cavity photons and the phonons. The position fluctuations of the phonon modes will be enhanced due to the amplification from the OPA, so in Fig.3 of  $S_b(\omega)$  we consider the following cases for the gain  $G$  of the optical parametric amplifier. When  $G = 0$ , the optical parametric amplifier is not active, meaning there is no amplification of the optical mode. In this case, the system is governed solely by the interaction between the cavity field and the YIG sphere through the magnetostrictive coupling. The spectrum  $S_b(\omega)$  which describes the fluctuations of the phonon mode, shows a single peak at  $G = 0$  (shown by Fig.3 red solid line). This indicates that the interaction is weak, and the normal mode splitting between the cavity and phonon modes is not yet prominent. The system behaves like a typical coupled cavity-mechanical system without gain, where the photon and phonon modes are not hybridized and behave as two uncoupled modes. Next when  $G > 0$  i.e. when the gain is increased slightly to  $G = 0.1\kappa_a$ , the OPA begins to amplify the optical mode in the cavity, thereby increasing the photon population. The increased number of photons strengthens the interaction between the cavity field and the mechanical mode phonons. However, at this low gain level, the coupling is not strong enough to fully enter the strong coupling regime, so the interaction remains moderate. In this case, the spectrum  $S_b(\omega)$  begins to show the early signs of normal mode splitting, but the splitting is not yet fully developed as shown by Fig.3 (Black solid line). we observe a slight broadening of the single peak or the beginnings of two closely spaced peaks, signaling the gradual hybridization of the photon and phonon modes. At  $G = 0.2\kappa_a$ , the gain of the OPA amplifies the optical mode further, resulting in a significant increase in the photon population within the cavity. This enhancement leads to a stronger coupling between the optical field and the phonons, pushing the system closer to the strong coupling regime. As a result, the position fluctuation spectrum  $S_b(\omega)$ , clearly exhibits two distinct peaks, representing the normal mode splitting as shown by Fig.3 (Blue dashed line). These two peaks correspond to the hybridized modes formed by the interaction between the photon and phonon modes. The splitting reflects the fact that the energy is now shared between the optical and mechanical modes, and the system has transitioned into a regime where the two modes are strongly coupled, exchanging energy efficiently. Furthermore When the OPA gain is increased to  $G = 0.4\kappa_a$ , the amplification of the optical mode is substantial, leading to a high photon population in the cavity. The interaction between the cavity field and the phonon mode is now so strong that the system is firmly in the strong coupling regime. The position fluctuation spectrum shows well-separated peaks, indi-

ating a significant normal mode splitting. The two peaks are farther apart compared to the lower gain cases, reflecting the high degree of hybridization between the optical and mechanical modes shown by Fig.3 (Red dashed line). The large separation between the peaks shows that the optical mode and the phonon mode are no longer independent, they have merged into two new hybrid modes with distinct frequencies, representing a complete redistribution of energy in the coupled system. This splitting grows with the effective coupling strength, which is strongly influenced by the OPA gain.

In Figure 4, we are going to visualize the output spectrum  $S_{\text{out}}(\omega)$  by analyzing the density plot, where the x-axis represents the normalized frequency  $\omega/\omega_b$  and the y-axis represents  $\Delta/2\pi$ . This density plot provides a clearer and more intuitive view of the changes in the output spectrum as the OPA gain increases. Notably, the most prominent feature observed in the output spectrum  $S_{\text{out}}(\omega)$ , is the normal mode splitting, which indicates the hybridization between the cavity mode and the phonon mode. When the gain is zero, the OPA is inactive, and the cavity field is not amplified. The system operates under normal interaction between the cavity mode and the mechanical mode of the YIG sphere, but the coupling is weak. The output field spectrum, which measures the spectral density of the light leaving the cavity, shows a single peak as shown in Fig.5(a). This peak reflects the optical response of the system, which is dominated by the cavity field, with minimal influence from the mechanical mode. In this weak coupling regime, the optical and mechanical modes are not mixed enough to form any noticeable splitting in the output spectrum. Further with the increment increase in gain to  $G = 0.1\kappa_a$  in Fig.4 (b), the system remains close to the weak coupling regime. By further increasing the gain of OPA to  $0.2\kappa_a$ , the output field spectrum  $S_{\text{out}}(\omega)$  now shows two distinct peaks clearly, indicating that the normal mode splitting has become visible, as shown in Fig.4(c). Moreover for  $G = 0.4\kappa_a$  the system is now in a regime where the cavity field at the output is strongly influenced by the presence of the mechanical mode, which shows two well-separated peaks as shown in Fig.4(d). These peaks correspond to the two hybridized modes formed by the intense interaction between the optical and phononic subsystems. The increased gain has amplified the coupling strength to the point where the energy exchange between the cavity mode and the phonon mode is efficient, and the two peaks are widely separated hence, the output spectrum is now a clear signature of the strong interaction in the presence of OPA gain.

#### A. Amplification and squeezing effects on output spectrum quadrature

The X and Y quadratures are crucial for analyzing the behavior of the cavity magnonics system with an optical parametric amplifier (OPA), as they reflect the delicate nature of amplification and squeezing effects. These quadratures represent the two orthogonal components of the output field, with the OPA typically amplifying the

Y quadrature while squeezing the X quadrature. This asymmetry highlights different aspects of photon-phonon interactions. By examining the spectra of both quadratures, we gain insights into the OPA's impact on the system's dynamics, particularly regarding normal mode splitting. Using equation 6, we plot the results as a density plot against normalized frequency and  $\Delta/2\pi$ , as illustrated in Fig. 5. For a gain of  $G = 0.4\kappa_a$ , we observe some squeezing in the X quadrature, resulting in narrower peaks in the spectrum, indicating suppressed noise or fluctuations in that quadrature, as shown in Fig. 5(a). As the OPA gain increases from  $G = 0.4\kappa_a$  to  $G = 0.6\kappa_a$ , noise suppression becomes more pronounced, resulting in sharper and narrower peaks in the X quadrature spectrum  $S_X(\omega)$ , as depicted in Fig. 5(b). At a gain of  $G = 1\kappa_a$ , the X quadrature experiences further squeezing, significantly reducing noise. The peaks in the X quadrature spectrum become even sharper and more defined, exhibiting narrower linewidths compared to lower gain values, indicating substantial fluctuation suppression, as shown in Fig. 5(c). When the gain is increased to  $G = 1.5\kappa_a$ , the X quadrature undergoes strong squeezing, leading to minimal noise in fluctuations. The spectrum's peaks are now sharply defined with very narrow linewidths, reflecting a level of squeezing that results in highly suppressed noise and well-defined spectral features, as illustrated in Fig. 5(d).

To examine the effects of the OPA on the Y quadrature, we apply equation (7) and plot the spectrum  $S_Y(\omega)$  as a density plot, illustrated in Fig. 6. In contrast to the X quadrature, the Y quadrature experiences anti-squeezing, leading to amplified noise. Consequently, the peaks in the Y quadrature spectrum are broader than those in the X quadrature at a gain of  $G = 0.4\kappa_a$ , indicating enhanced fluctuations as shown in Fig. 6(a). Additionally, at a gain of  $G = 0.6\kappa_a$ , the Y quadrature undergoes stronger anti-squeezing, resulting in further amplification of fluctuations. This leads to even broader peaks in the Y quadrature spectrum  $S_Y(\omega)$ , as shown in Fig. 6(b). When the OPA gain reaches  $G = 1\kappa_a$ , the strong anti-squeezing results in a noticeable broadening of the spectrum peaks. The increased fluctuations dominate, producing much broader features in the Y quadrature spectrum and indicating significant noise amplification, as illustrated in Fig. 6(c). At  $G = 1.5\kappa_a$ , the high parametric gain makes the effects of the OPA on the quadratures even more pronounced. In this case, the Y quadrature exhibits very strong anti-squeezing, leading to significantly amplified fluctuations and noisier peaks in the Y quadrature spectrum, reflecting substantial noise amplification, as shown in Fig. 6(d).

## B. Force Sensing

In this subsection, we aim to analyze the force sensing behavior of the system, focusing on the influence of an external force applied to the YIG sphere  $F_{ext}$ . This force is expected to interact primarily with the phononic modes, due to the magnetostrictive effects induced by the bias

magnetic field. By monitoring the phononic modes and their coupling to the cavity output field, we can gauge the system's sensitivity to external forces. Furthermore, we will present the expression for force sensitivity in this system, which we have calculated by considering both intrinsic thermal noise from the phononic modes and additional noise introduced through interactions with the cavity, particularly via the OPA and also by magnon. By analyzing these noises, we can quantify the force sensitivity. Here we define the force sensitivity  $S_F$  and can be calculated by taking the Fourier transform of equation (3) i.e.  $\delta\dot{a}$ ,  $\delta\dot{m}$ , and  $\delta\dot{b}$ , with quadrature  $\delta x = \delta a + \delta a^\dagger$ ,  $\delta y = i(\delta a^\dagger - \delta a)$ ,  $\delta X = \delta m + \delta m^\dagger$ ,  $\delta Y = i(\delta m^\dagger - \delta m)$ ,  $\delta u = \delta b + \delta b^\dagger$ ,  $\delta v = i(\delta b^\dagger - \delta b)$ , then by using the input output relation  $\delta y_{out} = \sqrt{2\kappa_a}\delta y - \delta y_{in}$  we can easily get the total added force. Where  $\delta_y$  is defined as

$$\delta_y = \frac{1}{s}\sqrt{2}(x_{ain}F_1 + y_{ain}F_2 + X_{min}F_3 + Y_{min}F_4 + g_{ap}u_{bin}F_5 + g_{ap}v_{bin}F_6 + (-F_{ext}g_{ap}F_7)) \quad (12)$$

In equation 10, the term  $F_1$ , and  $F_2$  is related to the cavity (Back action noise),  $F_3$ , and  $F_4$  is related to the noise from YIG,  $F_5$ , and  $F_6$ , are the thermal noise associated with the mechanics (phonons) and finally  $F_7$ , is related to the external force on the YIG. After solving the input output relation one can get the total added force  $F_{add}$ , however we will not present here the expression for that, because the full expression is a bit long and the expansion of this equation is omitted for clarity but can be derived by following the methodology in [45, 46] which follow standard procedures. So far To keep the main text focused, we present only the final form of the force sensitivity  $S_F$  by using

$$S_F(\omega)\delta(\omega - \omega') = \frac{1}{2}(\langle F_{add}(\omega) \rangle F_{add}(-\omega') + c.c) \quad (13)$$

In Fig. 7 the relationship between the OPA gain  $G$  and the system's sensitivity to external force is examined. Initially, as the OPA gain  $G$  is increased, we observe an enhancement in the force sensitivity of the system, reaching a maximum at a gain of  $0.46\kappa_a$ . This can be attributed to the amplification of the optical signal by the OPA, which increases the system's ability to detect small variations in the external force. In this region, the amplification provided by the OPA enhances the coupling between the YIG sphere's magnetization and the optical cavity's response, making the system more sensitive to force-induced shifts in the optical properties of the cavity. However, beyond a certain point, specifically at  $0.5\kappa_a$ , the force sensitivity begins to decrease. This reduction in sensitivity can be explained by the nonlinear behavior of the OPA at higher gain values. At higher gains, the system enters a regime where the amplified signal becomes more prone to noise and saturation effects. The OPA may begin to introduce distortions into the amplified signal, leading to a reduction in the precision with which small forces can be measured. Additionally,



the increase in gain can result in an imbalance in the optical cavity, where the amplification starts to overshadow the subtle force-induced changes, thereby diminishing the system's ability to resolve those changes effectively. The sensitivity to the external force is shown by the Red solid line in Fig. 7 when  $G = 0$ . By further increase in  $G$  i.e. when  $G$  is  $0.2\kappa_a$ ,  $0.3\kappa_a$ ,  $0.4\kappa_a$ ,  $0.46\kappa_a$  the sensitivity is further enhanced and is shown by the Blue, Black (solid line) and Blue, Black (Dashed) lines. The plot clearly illustrates that beyond  $G = 0.46\kappa_a$  the sensitivity begins to drop and is shown by the Red Dashed line.

## VII. Conclusion

In this work, we explored the behavior of a system comprising a single cavity containing an optical parametric amplifier and a YIG sphere subjected to a bias magnetic field, which generates phonons through magnetostrictive forces. We focused on analyzing the position fluctuation spectrum  $S_b(\omega)$ , the output field spectrum  $S_{out}(\omega)$ , and the quadrature spectra  $S_X(\omega)$  and  $S_Y(\omega)$ , with special attention to the effect of varying the OPA gain  $G$ . When the OPA gain was set to zero, the system exhibited a simple single-peak structure in both the mechanical and optical spectra, indicating weak interaction between the cavity photons and the phonons of the YIG sphere. However, as the OPA gain was gradually increased (e.g.,  $G = 0.1\kappa_a$ ,  $0.2\kappa_a$ ,  $0.4\kappa_a$ ), we observed the development of normal mode splitting in both  $S_b(\omega)$  and  $S_{out}(\omega)$ . This splitting is a clear signature of the enhanced coupling between the cavity field and the phonon mode, driven by the OPA-amplified photon population in the cavity. The increased OPA gain results in stronger energy exchange between the optical and mechanical subsystems, leading

to the hybridization of the cavity and phonon modes.

Further, the analysis of the  $X$  and  $Y$  quadrature of the output field revealed important sensitive effects introduced by the OPA. The  $Y$  quadrature, which is amplified by the OPA, exhibited more pronounced normal mode splitting due to the stronger interaction between the photons and phonons in this quadrature. In contrast, the  $X$  quadrature, which experiences squeezing, showed less splitting, as the reduced fluctuations suppressed the photon-phonon interaction. This asymmetry between the quadrature highlights the OPA's ability to selectively amplify or squeeze the field, influencing the coupling strength and modifying the optical response of the system.

Further, we have investigated the force sensitivity of this system in which the OPA gain plays a crucial role in determining the sensitivity of the system to external forces. Specifically, as the OPA gain  $G$  increases, the system's sensitivity to small external forces improves, with the optimal sensitivity observed at  $\kappa_a$ . However, further increases in the gain, particularly at  $0.5\kappa_a$  lead to a noticeable reduction in sensitivity. This reduction in sensitivity at higher OPA gains can be attributed to nonlinear effects and signal saturation within the OPA. While amplification initially enhances the system's ability to detect weak forces, excessive amplification introduces noise and distorts the optical signal, diminishing the precision of force measurements. Therefore, it is essential to carefully balance the OPA gain to maximize force sensitivity and avoid the adverse effects of signal saturation.

**Data Availability Statement** This manuscript has associated data in a data repository. All data included in this paper are available upon request by contacting with the corresponding author.

- 
- [1] M. Aspelmeyer, T. J. Kippenberg, and F. Marquardt, *Reviews of Modern Physics* **86**, 1391 (2014).
  - [2] J. B. Clark, F. Lecocq, R. W. Simmonds, J. Aumentado, and J. D. Teufel, *Nature* **541**, 191 (2017).
  - [3] C. Wang, L. Banniard, K. Brkje, F. Massel, L. Mercier de Lpinay, and M. A. Sillanpaa, *Nature Communications* **15**, 7395 (2024).
  - [4] J. Guo, R. Norte, and S. Gblacher, *Physical review letters* **123**, 223602 (2019).
  - [5] R. Nongthombam, A. Sahoo, and A. K. Sarma, *Physical Review A* **104**, 023509 (2021).
  - [6] J.-Y. Yang, D.-Y. Wang, C.-H. Bai, S.-Y. Guan, X.-Y. Gao, A.-D. Zhu, and H.-F. Wang, *Optics express* **27**, 22855 (2019).
  - [7] S. Huang and G. Agarwal, *Physical Review A—Atomic, Molecular, and Optical Physics* **80**, 033807 (2009).
  - [8] S. Gblacher, K. Hammerer, M. R. Vanner, and M. Aspelmeyer, *Nature* **460**, 724 (2009).
  - [9] M. Rossi, N. Kralj, S. Zippilli, R. Natali, A. Borrielli, G. Pandraud, E. Serra, G. Di Giuseppe, and D. Vitali, *Physical Review Letters* **120**, 073601 (2018).
  - [10] C. Ockeloen-Korppi, E. Damskgg, J.-M. Pirkkalainen, M. Asjad, A. Clerk, F. Massel, M. Woolley, and M. Sillanp, *Nature* **556**, 478 (2018).
  - [11] A. H. Safavi-Naeini, S. Gblacher, J. T. Hill, J. Chan, M. Aspelmeyer, and O. Painter, *Nature* **500**, 185 (2013).
  - [12] R. J. Thompson, G. Rempe, and H. J. Kimble, *Phys. Rev. Lett.* **68**, 1132 (1992).
  - [13] R. J. P. G, A. H. C. K. S, K. L. K. V. Reitzenstein, T. Reinecke, and F. A, *Nature* **432**, 197 (2004).
  - [14] T. Kumar, A. B. Bhattacharjee, and ManMohan, *Physical Review A—Atomic, Molecular, and Optical Physics* **81**, 013835 (2010).
  - [15] A. Tuchman, R. Long, G. Vrijsen, J. Boudet, J. Lee, and M. Kasevich, *Physical Review A—Atomic, Molecular, and Optical Physics* **74**, 053821 (2006).
  - [16] M. Raizen, R. Thompson, R. Brecha, H. Kimble, and H. Carmichael, *Physical review letters* **63**, 240 (1989).
  - [17] J. Klinner, M. Lindholdt, B. Nagorny, and A. Hemmerich, *Physical review letters* **96**, 023002 (2006).
  - [18] S. Huang and G. Agarwal, *Physical Review A—Atomic, Molecular, and Optical Physics* **81**, 033830 (2010).
  - [19] M. Asjad, *Journal of Modern Optics* **59**, 917 (2012).
  - [20] T. Wang, M.-H. Zheng, C.-H. Bai, D.-Y. Wang, A.-D.

- Zhu, H.-F. Wang, and S. Zhang, *Annalen der Physik* **530**, 1800228 (2018).
- [21] S. K. Singh, M. Mazaheri, J.-X. Peng, A. Sohail, Z. Gu, and M. Asjad, *Quantum Information Processing* **22**, 198 (2023).
- [22] S. Shahidani, M. Naderi, and M. Soltanolkotabi, *Journal of Modern optics* **62**, 114 (2015).
- [23] S. Barzanjeh, M. Naderi, and S. M., *Physical Review A—Atomic, Molecular, and Optical Physics* **84**, 063850 (2011).
- [24] X. Zhang, C. Zou, L. Jiang, and H. Tang, *Adv* **2**, e1501286 (2016).
- [25] X. Zuo, Z.-Y. Fan, H. Qian, M.-S. Ding, H. Tan, H. Xiong, and J. Li, *New Journal of Physics* **26**, 031201 (2024).
- [26] H. Huebl, C. W. Zollitsch, J. Lotze, F. Hocke, M. Greifenstein, A. Marx, R. Gross, and S. T. Goennenwein, *Physical Review Letters* **111**, 127003 (2013).
- [27] M. Goryachev, W. G. Farr, D. L. Creedon, Y. Fan, M. Kostylev, and T. M. E, *Physical Review Applied* **2**, 054002 (2014).
- [28] Y. Cao, P. Yan, H. Huebl, S. T. Goennenwein, and G. E. Bauer, *Physical Review B* **91**, 094423 (2015).
- [29] N. Bergeal, F. Schackert, M. Metcalfe, R. Vijay, V. Manucharyan, L. Frunzio, D. Prober, R. Schoelkopf, S. Girvin, and M. Devoret, *Nature* **465**, 64 (2010).
- [30] V. Fiore, Y. Yang, M. C. Kuzyk, R. Barbour, L. Tian, and H. Wang, *Physical review letters* **107**, 133601 (2011).
- [31] R. W. Andrews, R. W. Peterson, T. P. Purdy, K. Cicak, R. W. Simmonds, C. A. Regal, and K. W. Lehnert, *Nature physics* **10**, 321 (2014).
- [32] W. Liu, M. Abbas, S. H. Asadpour, H. R. Hamed, P. Zhang, and B. C. Sanders, *New Journal of Physics* **26**, 093042 (2024).
- [33] J. Li, S.-Y. Zhu, and G. Agarwal, *Physical Review A* **99**, 021801 (2019).
- [34] Y. Tabuchi, S. Ishino, A. Noguchi, T. Ishikawa, R. Yamazaki, K. Usami, and Y. Nakamura, *Science* **349**, 405 (2015).
- [35] A. Sohail, R. Ahmed, A. Shahzad, and M. A. Khan, *International Journal of Theoretical Physics* **61**, 174 (2022).
- [36] J. Li, S.-Y. Zhu, and G. Agarwal, *Physical review letters* **121**, 203601 (2018).
- [37] G. Din, M. Abbas, and P. Zhang, *The European Physical Journal Plus* **139**, 1 (2024).
- [38] S. Das, S. Chakraborty, and T. N. Dey, *Physical Review A* **108**, 033517 (2023).
- [39] M. Wang, D. Zhang, Y.-Y. Wu, T.-S. Yin, and Z.-Y. Sun, *arXiv preprint arXiv:1809.09309* (2018).
- [40] X.-Y. Zhang, C. Cao, Y.-P. Gao, L. Fan, R. Zhang, and C. Wang, *New Journal of Physics* **25**, 053039 (2023).
- [41] C. A. Potts, E. Varga, V. A. Bittencourt, S. V. Kusminskiy, and J. P. Davis, *Physical Review X* **11**, 031053 (2021).
- [42] C. Kittel, *Physical Review* **110**, 836 (1958).
- [43] M. O. Scully and M. S. Zubairy, *Quantum optics* (Cambridge university press, 1997).
- [44] E. X. DeJesus and C. Kaufman, *Physical Review A* **35**, 5288 (1987).
- [45] F. Bariani, H. Seok, S. Singh, M. Vengalattore, and P. Meystre, *Phys. Rev. A* **92**, 043817 (2015).
- [46] M. H. Wimmer, D. Steinmeyer, K. Hammerer, and M. Heurs, *Phys. Rev. A* **89**, 053836 (2014).